OPTICAL REVIEW Vol. 12, No. 4 (2005) 339–344

Serpentine Spring Corner Designs for Micro-Electro-Mechanical Systems Optical Switches with Large Mirror Mass

Guo-Dung John SU*, Shao Hsuan HUNG, Dexin JIA and Fukang JIANG[1]

National Taiwan University, Graduate Institute of Electro-Optical Engineering, 1 Roosevelt Road Sec. 4, Taipei, 106, Taiwan, R.O.C.

[1]*Umachines, Inc., 2400 N. Lincoln Avenue, Altadena, CA 91001, U.S.A.*

(Received October 18, 2004; Accepted January 31, 2005)

In this paper, we describe the design principles of serpentine springs with high reliability for the micro-electro-mechanical systems (MEMS) optical switches with large mirror mass. The most often seen failure mode of the MEMS optical switches under reliability tests is the breaking of these springs, which provide the restoring force for the MEMS actuators. The breaking points are usually at the turning corner of the serpentine springs when the MEMS optical switches are under a high G shock test or a vibration test. In order to overcome the difficulties, we redesigned the corner shapes of the springs with careful consideration. We will discuss the theoretical analysis and simulation modeling for the corner shapes of serpentine springs. MEMS optical switches with redesigned serpentine springs are fabricated and tested to prove the proposed design. The results show that the MEMS optical switches with new serpentine springs can pass rigorous reliability tests.

Key words: MEMS, optical switches, serpentine springs, corner effects, failure modes, reliability

1. Introduction

During the past few years, broadband communications and wireless access have made explosive progress in internet data traffic, which required the evolution of optical telecommunications networks for simple, quick and flexible applications. Optical crossconnect (OXC) switching technology provides a promising solution to realize high-capacity and high-complexity systems in the future. Transparent space-division optical switches are needed for rerouting optical signals in fiber networks. The requirements of such switches include low insertion loss, low crosstalk, wavelength independence and high power handling capability. Based on these criteria, it has been demonstrated that free-space micro-electro-mechanical system (MEMS) optical switches can provide satisfactory performance.[1–4)]

For large to medium port count optical MEMS switches, the arrangement of mirror arrays can be generally classified into either analog[5–7)] or digital[8–10)] approaches in terms of switching mechanism. The digital approach, also known as two-dimensional (2D) configuration, has the advantage of simpler position control over the analog approach. In the 2D arrangement, the optical path is parallel to the surface of wafer substrates and the length of the light path varies dependent upon switching ports. Additionally, the beam diameter of the light will gradually expand over a long traveling distance due to the diffraction of the light. As a result, the fiber coupling efficiency will be mainly determined by longitudinal misalignment, assuming minimal angular and lateral misalignment. The insertion loss due to longitudinal misalignment for a single mode fiber can be estimated by:

$$IL_{\text{long}} = -10\log\left(\frac{1}{Z^2+1}\right) \tag{1}$$

$$Z = \frac{x\lambda}{2\pi n_0 {w_0}^2},$$

where x is the longitudinal mismatch length, λ is the wavelength, n_0 is the refractive index of the air, and w_0 is the Gaussian beam waist. eq. (1) shows that the larger the beam diameter, the smaller the optical insertion loss due to longitudinal mismatch. Given the maximum 1 dB insertion loss, the range of misalignment length for the 200 μm beam diameter is close to 4 times larger than that of the 100 μm beam diameter. This shows that larger beam diameter has better performance in terms of longitudinal misalignment, which is important to 2D optical switches with different paths for various ports. To achieve good insertion loss in the 2D optical switches, the size of the reflecting micromirror must be at least several hundred micrometers to accommodate large beam diameters.

In addition to longitudinal misalignment, the curvature of the micromirror and surface roughness will degrade the optical performance. Free-space optical switches generally use single crystalline silicon or polysilicon mirrors. Due to the residual stress in polysilicon thin films,[11)] it is more desirable to use stress-free single crystalline silicon as a reflection surface. If the surface is not smooth, light is scattered, resulting in additional insertion loss. The total amount due to the scattering from the micromirror is estimated[12)] as:

$$P_{\text{scat}} = (1 - e^{-(4\pi\sigma\cos\theta_i/\lambda)^2})P_{\text{tot}}, \tag{2}$$

where P_{tot} is the total flux of incident light, P_{scat} is the flux of light scattered, λ is the wavelength, θ_i is the incident angle and σ is the surface roughness. Therefore, single crystalline silicon with smooth surface roughness would be a reasonable choice for a low insertion loss micromirror.

Based on the previous reasons, we conclude that the size and mass of the micromirrors will be big and heavy for 2D MEMS optical switches to achieve low insertion loss. This

*E-mail address: gdjsu@cc.ee.ntu.edu.tw

will be challenging to fabricate such two dimensional MEMS optical switches because we observed that the micromirrors required by most optical component manufactures fell off during the 500-G shock test. To overcome such difficulties without sacrificing the optical performance, the mechanical springs will need careful designing to hold micromirrors with large mass.

There are different types of spring designs. Serpentine springs with minimized stress for linear actuation[13] were shown to achieve large lateral displacement by shape memory alloys (SMA). A V-shaped torsion bar[14] was proposed to achieve a large rotational angle with lower driving voltage. Both spring structures are optimized to achieve larger displacement with less input power or lower actuation voltage. In this paper, we propose spring designs to pass severe reliability tests, such as shock, vibration and long-term cycling. In order to minimize the valuable layout space occupied by springs, we start with serpentine spring, which turns the straight bars into folded shapes. We will describe how to design serpentine springs with high reliability for micromirrors with a large and smooth reflecting area. In §2, we will discuss the theoretical analysis of serpentine springs. The fabrication and test results of MEMS optical switches will be given in §3. Finally, we will summarize the paper in the Conclusion section.

2. Theoretical Analysis and Simulation Results

Since the serpentine springs are made of single crystalline silicon, it is assumed that the material does not yield until fracture occurs. Originally, we assumed that the failure stress should be the fracture strength of silicon, which is approximately 7000 MPa.[15] This high yield contradicted our test results, where failure stresses are estimated to be less than the reported number. Sooriakumar tracked this discrepancy to the sharp corners introduced by anisotropic etching or structure shapes.[16] Therefore, stress concentration must be taken into careful consideration. In the following paragraphs, we will start with theoretical analysis to understand the stress distribution on serpentine springs. Detailed finite element methods (FEM) simulation results will be performed to verify the analytic considerations.

A schematic drawing of a micro actuator with a vertical micromirror is shown in Fig. 1. A vertical mirror made with single crystalline silicon is attached to the micro actuator flap to switch the light into the selected channel. The switch is actuated by electro-magnetic force. The metal coils are patterned on the actuation flap on the other side of the micromirror. Permanent magnets are attached underneath the actuation flap to provide an external magnetic field. When the current is applied to the metal coils on the actuation flap, the electro-magnetic force is generated to move the single-crystalline silicon mirror out of the cavity to reflect the light. The moving direction of the silicon micro mirrors is perpendicular to the silicon wafer substrate. The design of the micromirror is 500 μm high, 20 μm thick and 1200 μm long to ensure low optical insertion loss. In order to eliminate any possible stiction, the design does not use any mechanical stopper in the moving path of the micro actuator.

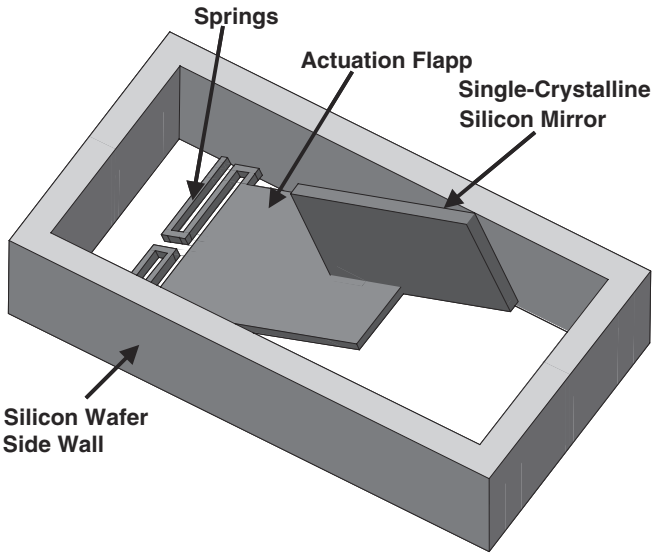

Fig. 1. Schematic drawing of a switching element of 2D MEMS optical switches.

The micro actuator is attached to the silicon sidewall with serpentine springs to save valuable layout space. However, the regular serpentine spring design makes the mechanical shock challenging because there is no mechanical structure to absorb shock or vibration energy applied to the micro actuators. In addition, the mass of the micromirror is larger than other reported MEMS optical switches made with polysilicon.[17–19]

To analyze the stress on the serpentine springs, we can resort to a membrane analogy.[20,21] The thickness of the membrane structure is small compared to surface dimensions and it thus has negligible bending rigidity. Imagine that a membrane is stretched over a cutout of the cross-sectional shape of a torsion bar. This analogy can simplify the procedure to find the stress function for folded torsion bars with various cross sections. The governing partial differential equation for deflection, w, of a membrane can be expressed as:

$$\frac{\partial^2 w}{\partial x^2} + \frac{\partial^2 w}{\partial y^2} = \frac{P_i}{N}, \tag{3}$$

where P_i is the constant tension force per unit area and N is constant tension force per unit length, which means how rigid the membrane is. Since the membrane is stretched over a cutout of the torsion bar, the directions of x- and y-axes are along the thickness and width of the torsion bar, respectively. The z-axis is not shown in the eq. (3), but it corresponds to length direction of the torsion bar. This analogy only applies to isotropic materials, but gives a good physical picture for stresses and is a good starting point to design proper serpentine springs.

Applying the membrane analogy to eq. (3), we can see a number of things. The location of maximum stresses is at the maximum slopes of the membrane, which corresponds to the corner of serpentine springs. The external corners do not add appreciably to the bending rigidity. So that most serpentine spring designs will smooth the inner corner at the bending of

the springs to relieve stress concentration. However, the stresses at the corner can be further reduced if one takes a closer look at the solution to eq. (3) for the case of the narrow rectangular cross-section, as shown in the following:

$$\sigma = \frac{2T}{J}x \qquad (4)$$
$$J = \frac{bt^3}{3},$$

where σ the strain, x the distance from the center of the torsion bar along the thickness, T the volume, b the width, and t the thickness of the torsion bar. Due to the MEMS fabrication process, the thickness of the whole serpentine springs will remain the same, but the designer can change the width of the corner to reduce the stress, which is proportional to the strain, to an acceptable level.

The above analysis can be further confirmed by FEM simulation using the commercial software ABAQUS. There are three different cases shown to explain the importance of the corner shape design. The first case of the regular serpentine spring is shown in Fig. 2(a), whose corner is sharp with a 90° fold. With the large slope at the inner corner, the maximum stresses around 717 MPa are concentrated. This makes the corners at serpentine springs vulnerable to high G shock. With rounded fillet (inner corner), the stress concentration can be significantly relieved to approximate 433 MPa (up to 30% reduction from the original design), as shown in Fig. 2(b). Based on the simulation result, we can tell that the stresses located at the corner do reduce due to the rounded fillet, but are still higher than the other parts of the serpentine springs. Figure 2(c) shows the stress distribution for the wider corners with the rounded fillet. By increasing the width of the turning corners, the stress can be further reduced to 401 MPa. From eq. (4) the width effect is small (linearly inverse proportional to the stresses), but this design can redistribute the maximum stresses over a much wider area along the torsion bar, instead of turning corners. The final design of a serpentine spring with longer length (more turns as well) is shown in Fig. 3. The torsion bar is 3000 µm long in total; its width at the straight part is 25 µm and the width at the corner is 50 µm. Compared with the serpentine spring in Fig. 2(a) which has no special design, the final design shows up to 80% stress reduction (from 717 to 119 MPa), which helps the MEMS optical switches with large masses pass a rigorous reliability test. The new design not only reduces the stress around the turning corners, but also redistributes the maximum stress from the turning corners to the straight parts of the torsion bar.

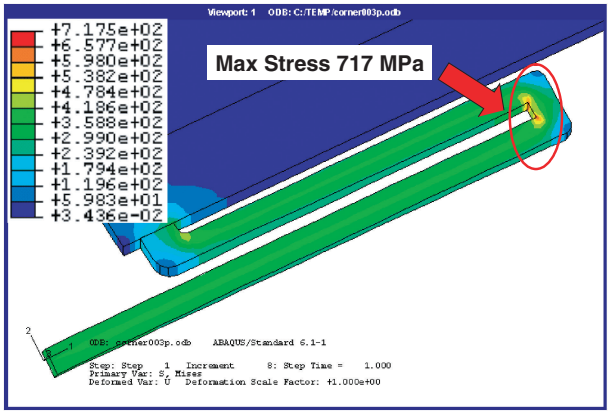

(a)

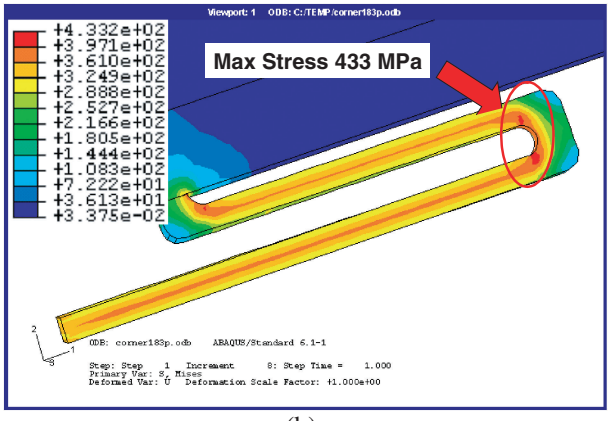

(b)

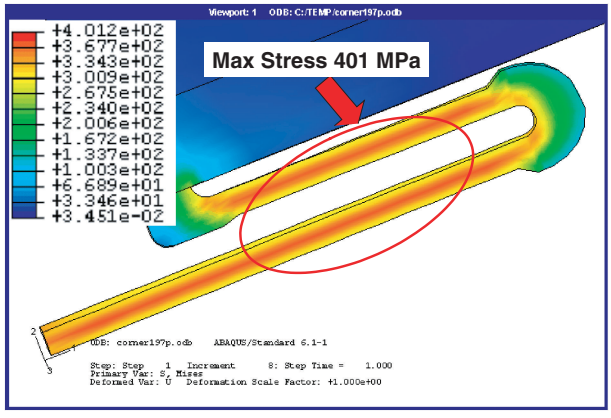

(c)

Fig. 2. FEM simulation results for serpentine springs with (a) sharp corner, (b)rounded inner corner, and (c) rounded inner corner and wide outer corner.

3. Device Fabrication Process and Experimental Test Results

To fabricate optical MEMS switches with smooth and vertical reflecting surfaces, we start with double-sided polished SOI wafers with the (110) substrate and the (100) device layer, which are fusion bonded together. LTO silicon dioxide was first deposited and patterned as the wet etching masks. Using anisotropic TMAH wet etching, vertical walls are created on the (111) planes of the substrate wafer and used as the reflecting mirror, as shown in step 2 of Fig. 4. The height of the fabricated micromirror is about 500 µm, the thickness is approximately 20 µm and the length is around 1200 µm. After the vertical mirrors were created, the gold was deposited by E-beam evaporator on the membrane and wet etched by gold etchant on the front side of the SOI wafer to create coils for generating electromagnetic force

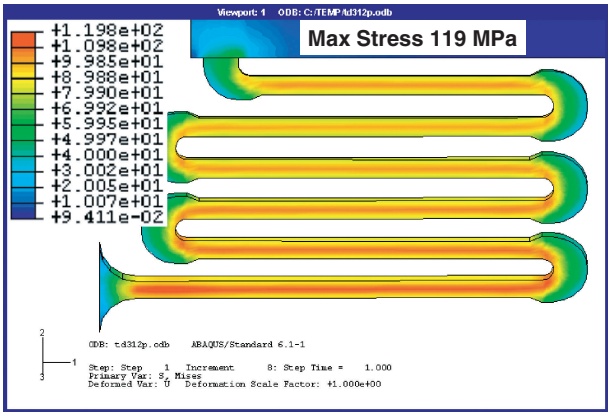

Fig. 3. The final design of a serpentine spring for 2D MEMS optical switches.

along with external magnetic fields provided by permanent magnets, as shown in step 3 of Fig. 4. Then the flap and serpentine springs were patterned by deep reactive ion etching (DRIE) on the device layer to release the micro-actuators. The turning corners of serpentine springs were made with the same shape as shown in Fig. 3. The scanning electron micrograph (SEM) picture in Fig. 5 shows the fabricated MEMS optical switches with detailed serpentine spring design. It can be clearly seen that the switching flaps with vertical mirrors are suspended in the air as a cantilever with minimum sticktion problem. The inner corners of the serpentine springs were rounded to minimize stress concentration. The width of the turning corner is increased to further reduce the stress concentration. The width of the corners is about twice of that of straight torsion bar.

Before the redesign of serpentine springs, the most often seen failure modes of shock/vibration tests of regular spring design were the broken microspring at the turning corners around 500 G shock, as the prediction in the FEM simulations shown in the §2. After redesigning the corner shape of the serpentine springs, we find that the broken parts are moved from the corners to the straight part of the springs, as shown in Fig. 6. The serpentine springs fail at approximately 1200 G mechanical shock.

With the newly designed serpentine springs, the fabricated devices went through rigorous reliability tests including shock, vibration and mechanical cycling, as described in the GR-1221 from Telcordia Technologies.[22] We performed the reliability tests on bare chips first to visually check whether the redesigned serpentine springs can meet the test requirements without any visible cracks under the high-resolution microscope. After that, chips selected randomly from other

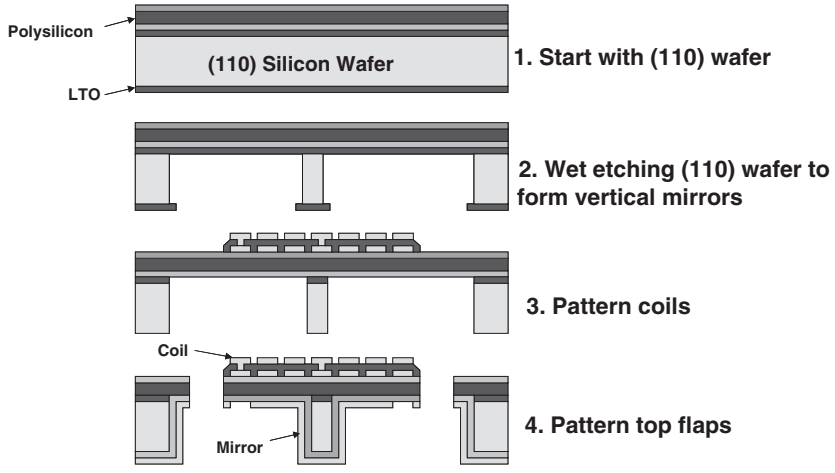

Fig. 4. Fabrication processes of MEMS actuators with large-surface vertical mirrors.

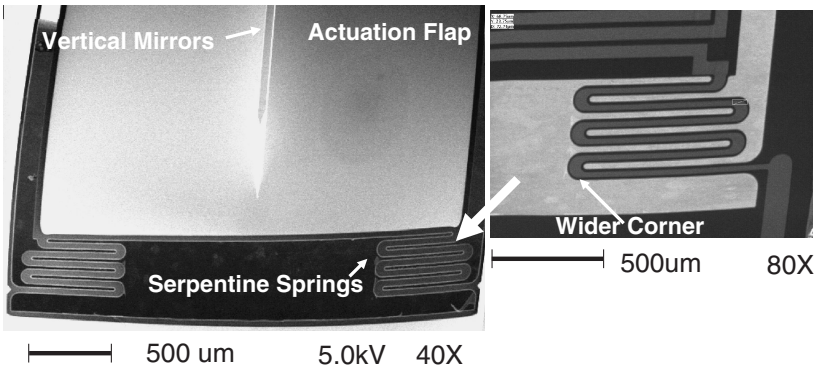

Fig. 5. SEM pictures of fabricated MEMS switches with detailed serpentine spring corner design.

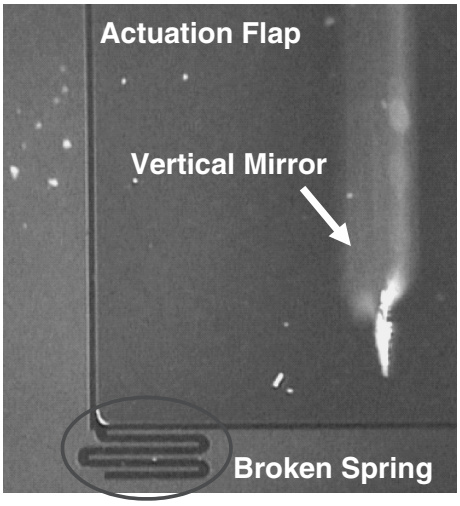

Fig. 6. A Photograph of a broken spring under a stereomicroscope.

fabrication batches were packaged with fiber collimators to verify the new spring design by optical insertion loss. The optical insertion loss of each package was measured before and after the tests with the same individual driving current. The passing criterion is that the delta insertion loss, measured before and after the test, should be less than ±0.5 dB according to GR-1221. Should any tiny crack occur on the springs, the delta insertion loss would be large after applying the same driving current because the optical alignment will have drifted away from the original optimized position.

In the mechanical shock, the test was performed in three mutually perpendicular axes, two directions in each axis and five times per direction. There were a total of 30 shocks for each optical switch. The amplitude of mechanical shock (impact) is 500 G with one milli-second duration. In order to attain meaningful statistic data, there were eleven samples subjected to the shock test to evaluate the redesigned serpentine springs. The results are shown in Fig. 7(a). The abscissa shows the delta insertion loss and the ordinate represents the pieces of samples. The maximum delta insertion loss is within ±0.3 dB and there are no samples that had failed after the shock test. This proves the newly designed spring corners passed the shock test.

The vibration test was done by mounting the samples on the vibration machine with an in-situ accelerometer in close loop control. The amplitude of the vibration was 20 G with the sweeping frequency from 10 to 2000 Hz and back to 10 Hz in 20 min. The test was performed 12 cycles per axis, in three mutual perpendicular axes. The final result is shown in Fig. 7(b) with all eleven pieces passing the test. Finally, we performed a long-term recycling test on the packaged switches. The switching speed was 20 Hz fully on and fully off switching cycles, (the switching time was less than 10 ms), which was monitored by optical power meters to ensure the switches were stable in each ON/OFF state. All eleven switches passed 100 million cycles without any failure, as shown in Fig. 7(c).

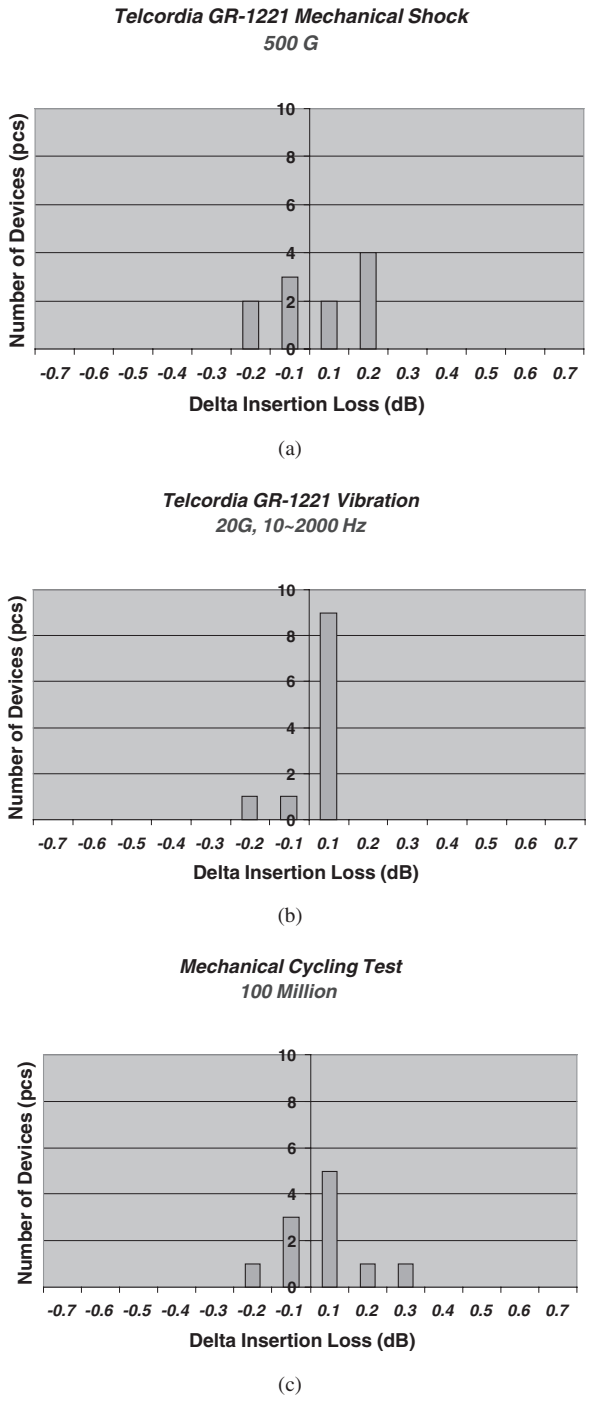

Fig. 7. Reliability tests for MEMS optical switches in (a) 500 G shock test, (b) 20 G vibration test from 10 to 2000 Hz and (c) 100 million switching cycling test.

4. Conclusion

In summary, we observed that the most-frequent failure mode of MEMS optical switches under the reliability test of Telcordia GR-1221 is the breaking of serpentine springs. From theoretical analysis, we realize that there is stress concentration in the fillet and this can be solved by redesigning the shape of serpentine springs on the layout level. We propose a rounded and wider corner design to lower the concentrated stress and move the maximum stress

away from the turning corners of the springs. The FEM simulation results of different corner designs are shown and discussed to verify the analysis. The MEMS optical switches with redesigned serpentine springs were fabricated and went through the reliability tests, including shock, vibration and recycling. The experimental results showed the switches with proposed serpentine springs passed the reliability test and proved the serpentine springs with wide-rounded corners meet expectations.

References

1) J. Ford, V. Aksyuk, J. Bishop and J. Walker: J. Lightwave Technol. **17** (1999) 904.
2) G. Su, F. Jiang, E. Chiu, A. Avakian, J. Dickson, D. Jia and T. Tsao: Proc. CLEO/PR, 2003, p. 96.
3) H. Toshiyoshi and H. Fujita: J. Microelectromech. Syst. **5** (1996) 231.
4) V. Aksyuk, D. Bishop and P. Gammel: U.S. Patent 5923798 (1999).
5) A. Neukermans and T. Slater: U.S. Patent 6044705 (1997).
6) A. Gasparan, V. Aksyuk, P. Busch and S. Arney: Proc. SPIE **4180** (2000) 86.
7) T. Yamamoto, J. Yamaguchi, R. Sawada and Y. Uenishi: NTT Tech. Rev. **1** (2003), No. 7, 37.
8) L. Lin, E. Goldstein and R. Tkach: IEEE Photonics Technol. Lett. **10** (1998) 525.
9) S. Lee, L. Lin and M. Wu: Electron. Lett. **31** (1995) 1481.
10) S. Lee, L. Huang, C. Kim and M. Wu: J. Lightwave Technol. **17** (1999) 7.
11) G. Su, H. Toshiyoshi and M. C. Wu: IEEE Photonics Technol. Lett. **13** (2001) 606.
12) C. Marxer, C. Thio, M. Gretillat, F. de Rooji, R. Battig, R. Anthamatten, O. Valk and P. Vogel: J. Microelectromech. Syst. **6** (1997) 277.
13) M. Kohl and K. D. Skrobanek: Proc. Transducers '97, Vol. 2, p. 785.
14) O. Tsuboi, Y. Mizuno, N. Koma, H. Soneda, H. Okuda, S. Ueda, I. Sawaki and F. Yamagishi: Proc. MEMS 2002, p. 532.
15) K. Petersen: Proc. IEEE **70** (1982) 420.
16) K. Sooriakumar: Electrochem. Soc. Proc. **95-27** (1995) 231.
17) A. Husain: Optical Fiber Communication Conf., 2001, keynote speaker.
18) A. Hussain and L. Fan: WIPO Patent 0073840, 2000.
19) L. Lin: OFC Tech. Dig., 1998.
20) R. Rivello: *Theory and Analysis of Flight Structure* (McGraw-Hill, New York, 1969).
21) S. Timoshenko and J. Goodier: *Theory of Elasticity* (McGraw-Hill, New York, 1970).
22) Reliability requirement for passive components, GR-1221, Telcordia Technologies, 1999, p. 6-1.